The impact of Secondary Ice Production on Arctic Stratocumulus

Georgia Sotiropoulou[1], Sylvia Sullivan[2], Julien Savre[3], Gary Lloyd[4], Thomas Lachlan-Cope[5], Annica M. L. Ekman[6], Athanasios Nenes[1,7]

[1]Laboratory of Atmospheric Processes and Their Impacts, School of Architecture, Civil & Environmental Engineering, École Polytechnique Fédérale de Lausanne (EPFL), Lausanne 1015, Switzerland
[2]Department of Earth and Environmental Engineering, Columbia University, New York, 10027, USA
[3]Meteorological Institute, Faculty of Physics, Ludwig-Maximilians-University, Munich, Germany
[4]Centre for Atmospheric Science, University of Manchester, Manchester, M139P, UK
[5]British Antarctic Survey, Cambridge, CB3 0ET, UK
[6]Department of Meteorology & Bolin Center for Climate Research, Stockholm University, Stockholm, 11419, Sweden
[7]Institute of Chemical Engineering Sciences, Foundation for Research and Technology-Hellas, Patras 26504, Greece

Correspondence to: georgia.sotiropoulou@epfl.ch, athanasios.nenes@epfl.ch

Abstract. In-situ measurements of Arctic clouds frequently show that ice crystal number concentrations (ICNCs) are much higher than the available ice-nucleating particles (INPs), suggesting that Secondary Ice Production (SIP) may be active. Here we use a Lagrangian Parcel Model and a Large Eddy Simulation to investigate the impact of three SIP mechanisms (rime-splintering, break-up from ice-ice collisions and droplet-shattering) on a summer Arctic stratocumulus case observed during the Cloud Coupling And Climate Interactions in the Arctic (ACCACIA) campaign. Primary ice alone cannot explain the observed ICNCs, and droplet-shattering is an ineffective SIP mechanism for the conditions considered. Rime-splintering, a mechanism that usually dominates within the studied temperature range, is also weak owing to the lack of large droplets to initiate this process. In contrast, break-up enhances ICNCs by 1-1.5 orders of magnitude, bringing simulations in good agreement with observations. Combining both processes can further explain some of the largest ICNCs observed. The main conclusions of this study show low sensitivity to the assumed INP and Cloud Condensation Nuclei (CCN) conditions. Our results indicate that collisional break-up may be an important ice-multiplication mechanism that is currently not represented in large-scale models. Finally, we also show that a simplified treatment of SIP, using a LPM constrained by a LES and/or observations, provides a realistic yet computationally efficient description of SIP effects that can eventually serve as an efficient way to parameterize this process in large-scale models.

1. Introduction:

Mixed-phase clouds are a critical component of the Arctic climate system due to their warming effect on the surface radiation balance (Shupe & Intrieri, 2004; Sedlar et al., 2011) and potential impact on the melting of sea ice. These clouds are very frequent in the summer, when they occur about 80–90% of the time and can persist for days to weeks (e.g. Shupe et al., 2011). However, their representation in

mesoscale and large-scale numerical weather prediction and climate models remains elusive (Karlsson and Svensson, 2013; Barton et al., 2014; Wesslén et al., 2014; Sotiropoulou et al., 2016).

An accurate description of mixed-phase clouds in models requires a solid knowledge of the amount and distribution of both liquid water and ice (e.g., Korolev et al., 2017). Ice crystals and liquid
45 drops form upon preexisting aerosols, termed ice nucleating particles (INP) and cloud condensation nuclei (CCN), respectively. However, the observed ice crystal number concentration (ICNC) can be orders of magnitude higher than the INPs (e.g., Rangno and Hobbs, 2001; Gayet et al., 2009; Schwarzenboeck et al., 2009; Lloyd et al., 2015). The enhanced ICNCs are especially surprising in the high Arctic, which is relatively clean and INPs are sparse (Gayet et al., 2009; Morrison et al. 2012).
50 Secondary Ice Processes (SIP) are suggested as the cause to explain this cloud-ice paradox (e.g., Gayet et al., 2009; Lloyd et al., 2015). SIP refers to a variety of collision-based processes that multiply the concentration of ice crystals in the absence of additional INP (e.g. Field et al., 2017, and references therein). Yet these processes are poorly represented in atmospheric models, resulting in potential errors in the representation of the surface shortwave radiation budget (Young et al., 2019).

55 The SIP processes known and studied to date include rime-splintering, break-up from ice-ice collisions and droplet-shattering. Rime-splintering (RS) is by far the most explored of all SIP mechanisms, and refers to the production of ice splinters after super-cooled droplets rime onto small graupel (Hallett and Mossop, 1974). This process occurs effectively for temperatures between -3 and -8°C (Hallett and Mossop, 1974; Heymsfield and Mossop, 1978), when liquid droplets smaller than 13
60 μm and larger than 25 μm are present (Hallett and Mossop, 1974; Choularton et al., 1980). RS is the only SIP mechanism that has been extensively implemented in weather prediction (e.g. Li et al. 2008; Crawford et al. 2012; Milbrandt and Morrison 2016) and climate models (e.g. Storelvmo et al. 2008; Gettelman et al. 2010).

Secondary ice production also occurs from collisions between ice crystals (Vardiman, 1978;
65 Takahashi et al., 1995) that lead to their fracturing and eventual break-up (BR). This mechanism is most effective at colder temperatures than required for RS, around -15◦C (Mignani et al. 2019). There is still little quantitative understanding regarding this mechanism and its dependence on atmospheric and cloud conditions; whatever is known comes from limited laboratory experimental data (Vardiman, 1978; Takahashi et al., 1995) and small-scale modeling (e.g. Fridlind et al., 2007; Yano and Phillips, 2011;
70 2016; Phillips et al, 2017a,b; Sullivan et al., 2017; 2018a). Relatively few attempts have been made to incorporate this process in mesoscale models (Hoarau et al. 2018; Sullivan et al. 2018b).

Recent laboratory studies suggest that ice multiplication at temperatures around -15°C can also occur from shattering of droplets with diameters between 50 and 100 μm (Leisner et al., 2014; Wildeman et al., 2017; Lauber et al., 2018) with presumably at least one INP that initiates the ice
75 formation process. Drop-shattering (DS) has been studied with small-scale models (Lawson et al., 2015; Sullivan et al., 2018a; Phillips et al., 2018) and found to be important for a range of atmospheric

conditions. Sullivan et al. (2018b) implemented parameterizations for DS and BR mechanisms in the COSMO-ART mesoscale model, which resulted in reduced discrepancies between modeled and observed ICNCs.

80   The thermodynamic conditions that favor the above mechanisms frequently occur in the Arctic. In this study, we examine the role of SIP during the Cloud Coupling And Climate Interactions in the Arctic (ACCACIA) flight campaign in 2013. Observations of stratocumulus clouds from the summer flights indicate that ICNCs were orders of magnitude higher than the measured aerosol concentrations that can act as INP, suggesting that ice multiplication may have taken place (Lloyd et al., 2015). To

85   investigate this hypothesis, we use a Lagrangian Parcel Model (LPM) that includes SIP descriptions and a Large Eddy Simulation (LES) that provides a realistic representation of the boundary-layer turbulence and thermodynamic conditions.

2. ACCACIA

90

2.1 Measurements

The ACCACIA flight campaign took place during March, April and July 2013, in the vicinity of Svalbard, Norway. The main objectives of this campaign were to reduce uncertainties regarding microphysical processes in Arctic clouds and their dependence on aerosol properties. For this purpose,

95   an extensive suite for microphysical and aerosol instruments was deployed (Lloyd et al., 2015; Young et al., 2016). Below, we offer a brief summary of the dataset utilized in this study.

Images of cloud particles collected with a two-dimensional Stereoscopic Probe (2D-S) at 10-μm resolution were used to calculate number concentrations and discriminate particle phase. The measured concentrations were fitted with "antishatter" tips (Korolev et al., 2011, 2013) to mitigate particle

100   shattering on the probe and have further been corrected for shattering effects using inter-arrival time (IAT) post analysis (Crosier et al. 2013). Ice Water Content (IWC) was determined from these data, using the Brown and Francis (1995) mass dimensional relationship: IWC is the sum of the masses of all ice particles recorded by the 2D-S probe, where the mass of each particle is estimated as a function of its diameter.

105   A DMT Cloud Droplet Probe (CDP) measured the liquid droplet size distribution between 3-50 μm and was used to derive Liquid Water Content (LWC). A GRIMM Portable Aerosol Spectrometer provided aerosol size distributions within the range 0.25-32 μm. Owing to a lack of direct INP measurements, GRIMM data was used to derive INP estimates by applying the DeMott et al. (2010) parameterization for primary ice nucleation. These estimates are obtained from aerosol concentrations

110   with diameter larger than 0.5 μm. Basic meteorological measurements (e.g. pressure, temperature, relative humidity with respect to ice) were also provided by Goodrich Rosemount probes.

Previous analyses of ACCACIA observations have shown that ice multiplication, associated with

enhanced ICNC, likely took place in summer, while ice production in springtime mixed-phased clouds
was likely driven by primary ice nucleation (Lloyd et al., 2015). For this reason, our study focuses on a
115   summer single-layer stratocumulus case observed on 23 July.

2.2 Case study

The data used in this study were collected on July 23, during Flight M194, when the aircraft flew on
120   northerly and southerly headings through a single-layer stratocumulus around 15°E, between 78.2 and
82°N. On this day, a low-pressure system was centered on 85°N 150°W, while high-pressure systems
were prevailing in the sampled region, with particularly high pressure over the north of Norway. Flight
M194 sampled clouds in the trailing low pressure system. Winds were usually from the west: the
aircraft sampled mostly downdrafts, ~5 m s^{-1}, when flying at ~1 km height and weak updrafts, ~2 m s^{-1},
125   above 2 km. A detailed description of the large-scale conditions can be found in Jones et al. (2018).

In this study, we focus on a single stratocumulus deck observed between 10-11 UTC, when the
aircraft was flying between 80.8-82°N and 14.7-15.3°E (Fig. 1). This case study is chosen as the aircraft
flew at relatively low altitudes, providing detailed information about the planetary boundary layer
(PBL) structure. During this period a temperature inversion was found between 0.8 km and 1.2 km
130   altitude, about 3°C strong (Fig. 2a). A specific humidity inversion co-existing with the temperature
inversion was also observed, with a strength of 0.5 g kg^{-1} (Fig. 2b). CDP measurements further indicate
the presence of a stratocumulus layer, about 450 m deep, the cloud top residing within the temperature
inversion. Such clouds that penetrate the temperature inversion layer are very frequent in the Arctic
(Sedlar et al. 2012). Finally, the cloud droplet number concentration (N_C) observed within this hour was
135   highly variable, ranging from 0.2 to 68 cm^{-3} (Fig. 2d), while the mean profile peaks at 30 cm^{-3}.

3.   Models and Methods

For our investigations we use a LPM specifically developed for the study of SIP (Sullivan et al., 2017;
2018a) and the MISU/MIT Cloud and Aerosol (MIMICA) LES (Savre et al., 2015), designed for the
study of Arctic clouds. The LPM allows a detailed description of the formation, growth and evolution of
140   cloud droplets and ice particles as they interact with each other, including SIP processes: RS is
described following Hallet and Mossop (1974), BR is described with a temperature-dependent
formulation based on the laboratory results in Takahashi et al. (1995) and DS is the same as in Sullivan
et al. (2018a). However, this model does not account for interactions of the cloudy updrafts with their
surrounding environment.

145   The LES provides a three-dimensional description of the cloud system at a high spatial and temporal
resolution, which is of similar scale as the observations. MIMICA does not include any SIP processes,
so the LPM – informed by the LES - is used to quantify the enhancement in ICNCs due to SIP
compared to primary ice formation. The ice crystal concentration in the LES (which includes only a

description of primary ice) is then enhanced by the LPM result. This coupling between the LES and
150 LPM occurs throughout the simulation. A detailed description of these modeling components and the
overall modeling methods and set-up are described below.

3.1 Large Eddy Simulation (LES)

The MIMICA LES (Savre et al., 2015) solves a set of non-hydrostatic prognostic equations for the
conservation of momentum, ice-liquid potential temperature and total water mixing ratio with an
155 anelastic approximation. A 4th order central finite-differences formulation determines momentum
advection and a 2nd order flux-limited version of the Lax-Wendroff scheme (Durran, 2010) is
employed for scalar advection. Equations are integrated forward in time using a 2nd order Leap-Frog
method and a modified Asselin filter (Williams, 2010). Sub-grid scale turbulence is parameterized using
the Smagorinsky-Lilly eddy-diffusivity closure (Lilly, 1992) and surface fluxes are calculated according
160 to Monin-Obukhov similarity theory.

Cloud microphysics are described using a two-moment approach for cloud droplets, rain and ice
particles. Mass mixing ratios and number concentrations are treated prognostically for these three
hydrometeor classes, whereas their size distributions are defined by generalized Gamma functions.
Cloud/rain droplet processes are treated following Seifert and Beheng (2001), while liquid/ice
165 interactions are parameterized following Wang and Chang (1993). A simple parameterization for CCN
activation is applied (Khvorostyanov and Curry, 2006), where the number of cloud droplets formed is a
function of supersaturation and CCN concentration. Ice nucleation is also parameterized following
Morrison et al. (2011): if ICNCs fall below the prescribed INP concentration (N_{INP}), they are nudged
upward towards the INP value. CCN and INP concentrations are passively advected within the model
170 domain and not depleted through droplet activation or ice nucleation processes. A detailed radiation
solver (Fu and Liou, 1992) is coupled to MIMICA to account for cloud radiative properties when
calculating the radiative fluxes.

All simulations are performed on a 96×96×128 grid, with constant horizontal spacing dx = dy =
62.5 m. The simulated domain is 6×6 km^2 horizontally and 1.77 km vertically. At the surface and in the
175 cloud layer the vertical grid spacing is 7.5 m, while between the surface and the cloud base it changes
sinusoidally, reaching a maximum spacing of 25 m. The integration time step is variable, calculated
continuously to satisfy the Courant-Friedrichs-Lewy criterion for the Leap-Frog method. Lateral
boundary conditions are periodic, while a sponge layer in the top 500 m of the domain damps vertically
propagating gravity waves spontaneously generated during the simulations. To accelerate the
180 development of turbulent motions, the initial ice-liquid potential temperature profiles are randomly
perturbed in the first 20 vertical grid levels with an amplitude not exceeding 0.0003 K.

3.2 Lagrangian Parcel Model (LPM)

The ice enhancement from SIP is estimated with an LPM with six hydrometeor classes for small,

185   medium, large ice and liquid hydrometeors (Sullivan et al., 2017; 2018a). Although the bin microphysics is coarsely resolved, it has served as a convenient framework for the study of ice multiplication, and especially the BR process (Yano and Phillips, 2011; Sullivan et al., 2018a).

The six hydrometeor number tendencies are solved with an explicit Runge-Kutta pair for delay differential equations (Bogacki and Shampine, 1989) and coupled to moist thermodynamic equations for pressure, temperature, supersaturation, liquid water and ice mixing ratios, and hydrometeor sizes;

190   the latter are solved with a second-order Rosenbrock solver (Rosenbrock, 1963). CCN activation is represented in the same way as in the LES. An INP nucleation rate is prescribed so that the LPM nucleates the same number of INPs as in the LES within the first three seconds of simulation. Each hydrometeors type resolved is represented by a characteristic size that is allowed to dynamically vary over time as a function of temperature and supersaturation. Ice hydrometeors are modeled as prolate

195   spheroids to account for their non-sphericity as in Jensen and Harrington (2015).

The characteristic major axis or radius for the LPM bins are 5 μm, 50 μm and 200 μm for the small, medium and large ice particles (e.g. graupels), respectively, and 1 μm, 12 μm, 25 μm for small, medium and large liquid droplets. The number in these classes is denoted N_i, N_g, N_G and N_d, N_r, N_R respectively. A typical timescale for ice crystals to grow to medium sizes (τ_i) for convective clouds with

200   updraft velocities $W \sim$ 2-3 m s^{-1} and cloud base temperature T_{cbh} = 0°C is 7.5 minutes (Sullivan et al. 2017). However, a somewhat longer τ_i is expected (~9 min) in Arctic stratocumulus conditions with T_{cbh} = -5°C and $W \sim$ 0.75 m s^{-1} (Sullivan et al. 2017). Although the colder T_{cbh} promotes ice crystal growth, the weaker updrafts have a pronounced opposing effect. Hence for our ACCACIA case, with mean $W \sim$0.25 m s^{-1} and mean T_{cbh}=-3.5°C, i.e. weaker vertical motions and warmer temperatures than in the

205   Arctic case in Sullivan et al. (2017), it is reasonable to assume an even slower $\tau_i \sim$12.5 min.

The timescale for medium ice particles (e.g. graupel) to grow to large ones (τ_g) can be inferred from the measurements, since the 2D-S instrument can trace ice particles larger than 75 μm. Ice particles with diameters 400 μm or larger are found systematically and at relatively larger concentrations above 830 m (Fig. S1), hence ~260 m above the cloud base height. The estimated time

210   for a cloud particle with a mean updraft velocity 0.25 m s^{-1} to reach this level, ascending from the cloud base is ~17.5 min. Hence a τ_g=17.5 min is assumed in our LPM simulations, somewhat faster than the timescale adopted in Sullivan et al. (2017).

A similarly empirical determination of the fallout timescale τ_G of the large ice particles is not possible. For their idealized Arctic simulation, Sullivan et al. (2017) adapted a timescale of τ_G=12.5

215   min. In our simulations, we tested three timescales: 12.5 min, 17.5 min and 22.5 min. Our results showed no sensitivity to these values. The simulations with τ_G=17.5 min are presented in the main text.

The timescale τ_d for small droplets to grow to medium ones is set to 5 min, based on Sullivan et al. (2017; 2018a). The timescale τ_r for medium drops to grow to large ones is constrained based on the LES simulations. The LES produces very few rain droplets with diameters greater 25 μm; the maximum

220   raindrop concentration never exceeds 0.15 cm^{-3} in the LES (Fig. S2a). For consistency, a relatively long

growth timescale is adapted, τ_r=26.7 sec, which allows for a limited number of droplets to grow to large

sizes, comparable to the LES results (Fig. S2b). This set-up is in general agreement with the observation

that very few droplets of diameters > 25 μm were found near cloud top over the ice-pack. The fallout

time τ_R of large rain droplets in the LPM is set to 30 min, the end of the simulated time, as very limited

225   precipitation (generally < 0.1 mm day^{-1}) is produced in the LES simulations.

Secondary ice processes in the LPM include: (a) RS, when a medium or large ice particle

collides with a large droplet, (b) BR, when a medium ice hydrometeor collides with a large one and (c)

DS, if a raindrop freezes. These processes are included in an ice generation function along with primary

ice nucleation (denoted as NUC below):

$$G_{ice} = \left.\frac{dN_i}{dt}\right|_{NUC} + \left.\frac{dN_i}{dt}\right|_{RS} + \left.\frac{dN_i}{dt}\right|_{BR} + \left.\frac{dN_i}{dt}\right|_{DS} =$$

230    $$= N_{INP} + F_{RS}[K_{RSg}N_g + K_{RSG}N_G] + F_{BR}K_{BR}N_gN_G + F_{DS}K_{BR}N_R$$

where K_X is the gravitational collection kernel and F_X the fragment number generated by process X

(where X=RS, BR, DS; in the case of RS – we consider both RS from small graupel, RSg and large

graupel, RSG). The fragment number generated by rime-splintering is formulated on the basis of the

laboratory experiments conducted by Hallet and Mossop (1974), who found a maximum of 360

235   splinters per milligram of rime generated round -5°C.

$$F_{RS} = 360\rho_w\frac{\pi}{6}(2r_R)^3 ,$$

where ρ_w is the water density and r$_R$ represents the radius of the large droplet. This process is fully

efficient in the temperature range of -4 to -6 ^{o}C, while its efficiency is decreased by 50% for

temperatures between -8 – -6 ^{o}C and -4 – -2 ^{o}C, and set to 5% below the optimal zone (Ferrier 1994).

240   The work of Takahashi et al. (1995) is used to describe break-up:

$$F_{BR} = 280(T - 252)^{1.2} e^{-(T-252)/5}$$

Droplet shattering is described as function of a freezing prbability (p_{fr}), parameterized following

Paukert et al. (2017), and a shattering probability (p_{sh}) based on droplet levitation experiments

245   conducted by Leisner et al. (2014):

$$F_{DS} = 2.5\cdot10^{-11}(2r_R)^4 p_{fr}p_{sh}$$

Freezing is allowed only when raindrop size exceeds 100 μm and p_{sh} is a normal distribution centered at

-15°C with a standard deviation of 10°C.

250   The number balance in each class is the generation function at the current time as a source and

the generation function at a time delay as the sink, along with aggregation and coalescence processes.

Note that aggregation occurs between small and medium ice particles and generates new particles in the largest bin. Similarly, coalescence removes droplets from the small and medium bins and generates new ones in the large raindrop category. A schematic of all these processes is shown in Fig. 3.

255   Finally, the hydrometeor number tendencies are coupled to the moist thermodynamic equations to account for the changing system supersaturation and thus changes in their size. All LPM equations are described in detail in Sullivan et al. (2017, 2018a).

3.3   Initial and boundary conditions

The atmospheric profiles used to initialize the LES are based on in-situ observations collected between

260   10-11 UTC on 23 July (Fig. 2), along the flight track shown in Fig. 1. The fact that the aircraft did not sample vertically through the atmosphere, but flew across a relatively large domain (9 km × 180 km) and over variable surface conditions (Fig. 1), induces some challenges for the design of the control simulation: measurements below the cloud layer and above the temperature inversion (Fig. 2a) are collected over the ocean, whereas the cloud layer is mostly sampled over the marginal-ice zones (MIZ)

265   and the ice-pack. However, the uncertainty arising from utilizing all these measurements to construct the initial vertical profiles (Fig. 2) is not necessarily larger than utilizing reanalysis data at a similarly coarse resolution.

Since our focus is on the cloud layer, we simulate ice-covered surface conditions in the LES. The co-existent temperature and specific humidity inversions, associated with the cloud top height, as

270   observed in Fig. 2, are typical characteristics of the summertime Arctic PBL (Sedlar et al., 2011; Tjernström et al., 2012) over sea-ice. However, as cloud characteristics can vary depending on the surface type, open-water, MIZ or thicker ice (Jones et al., 2017), we only use cloud measurements collected at latitudes higher than 81.7°N (Fig. 1) and within a 9×33 km ice-covered area to evaluate the simulated cloud properties.

275   The wind forcing is set by specifying the geostrophic wind, constant with height, equal to the observed vertical mean value of 5.8 m s^{-1}. The surface pressure is set to 1010 hPa, linearly extrapolated from low-level pressure measurements. The surface temperature is set to 0°C and surface moisture to the saturation value, which reflect summer ice conditions. Surface albedo is set to 0.65, representative of the sea-ice melting season (Persson et al., 2002). In MIMICA, subsidence is treated as a linear

280   function of height: $w_{LS} = -D_{LS}z$, where D_{LS} is the large-scale divergence. D_{LS} here is defined through trial and error: to avoid rapid vertical cloud displacements, we prescribe $D_{LS} = 8*10^{-6}$ s^{-1}.

A N_{CCN} concentration of 50 cm^{-3} is prescribed, based on measurements of cloud droplet concentrations over the ice-pack (Fig. 2d). The mean observed INP concentration is 0.006 L^{-1} and never exceeds 0.05 L^{-1}, while the mean and maximum observed ICNC for the same period is 1.43 L^{-1} and 17.8

285   L^{-1}, respectively, suggesting substantial ice multiplication. Selecting INP = 0.01 L^{-1} results in the development of a purely liquid cloud layer in the LES (see Section 4.3). Given that the uncertainty in

the DeMott parameterization is about one order of magnitude (DeMott et al., 2010), we therefore assume a baseline simulation where INP= 0.1 L^{-1} which generally constitutes an upper bound based on existing measurements in the Arctic (Wex et al., 2019). However, the sensitivity of the results to both

290   CCN and INP assumptions will be discussed in detail in Sections 4.2 and 4.3.

Initial specific humidity and pressure in the LPM are set to the values measured at the cloud base (3.1 g kg^{-1} and 980 hPa, respectively). The LPM is then run over a wide temperature and vertical velocity range to encompass the in-cloud variability encountered during the LES simulation. Given that the mean W in the LES simulation is 0.25 m s^{-1} and the simulated cloud depth is 450 m (Fig. 2c), the

295   cloud mixing timescale is about 30 minutes – so all LPM simulations are run for 30 minutes at maximum. A simulation also stops earlier if the parcel reaches the lowest cloud temperature observed near cloud top, -6.5°C. With this condition we ensure that parcels with larger velocities do not reach colder temperatures in the LPM than those encountered in the cloud simulated by the LES.

The ice enhancement factors, defined as N_{ice}/N_{INP}, where N_{ice} is the sum of ice number

300   concentrations in all 3 bins, are derived from the LPM calculations at the end of the simulation time. These factors are saved in look-up tables and then used by the LES: the ICNC in each LES column is multiplied at each model time-step by an enhancement factor, which is a function of the cloud base temperature (T_{cbh}) and the mean cloud updraft velocity (W).

3.4   Sensitivity experiments

305   The relative contribution of the different SIP mechanisms during the ACCACIA case is quantified through a number of sensitivity simulations. Initially, we run the LPM for four different set-ups with: (a) RS, (b) BR, (c) DS being the only active mechanism, and with (d) all known SIP mechanisms activated. The LPM simulations suggest that RS and BR can play a critical role in Arctic stratocumulus conditions, while DS remains inactive (not shown), consistent with previous studies that have shown

310   that a relatively warm cloud base temperature is critical for the initiation of DS (Lawson et al., 2017; Sullivan et al., 2018a). These results are then used to parameterize the SIP effect in the LES through look-up tables (see Section 3.3). In addition to the control simulation (CNTRL), which does not account for any ice multiplication, three LES sensitivity experiments are conducted, which are referred to as (a) RS, (b) BR and (c) ALLSIP in the text, to reflect the SIP mechanism(s) that contribute(s) to ice

315   multiplication. The DS mechanism is not further investigated with the LES.

Since there are many uncertainties related to the N_{CCN} and INP concentrations prescribed in the control experiments, we carry out two additional sets of sensitivity simulations. The first set accounts for variations in N_{CCN} by prescribing two different concentrations: 10 cm^{-3} and 100 cm^{-3}. This range covers a variety of atmospheric conditions, from very pristine to cases where polluted air has been

320   advected form the south. Note that CCN can be highly variable in the Arctic, typically spanning the range 10-300 cm^{-3} within the PBL (Jung et al., 2018). Two different set-ups are used for these tests: (a)

similar to the CNTRL simulation with no ice multiplication and (b) all SIP mechanisms activated. These LES simulations are referred to as (a) CCN10 and CCN100, and (b) CCN10_SIP and CCN100_SIP.

325   The second set of simulations includes variations in the prescribed INP. Note that INPs in the Arctic are sparse, hardly ever exceeding 0.1 L^{-1} (Wex et al., 2019). Aerosol measurements of the ACCACIA case study indicate a mean (max) INP concentration of 0.006 L^{-1} (0.05 L^{-1}). Considering these variations, two INP values are tested, smaller/ larger by an order of magnitude compared to the control experiment: 0.01 L^{-1} and 1 L^{-1}. Again, the two different set-ups are applied, resulting in four

330   sensitivity simulations: IN0.01, IN1, IN0.01_SIP and IN1_SIP. A summary of all LES experiments is offered in Table 1. All simulations are run for 8 hours; the first 4 hours are considered as spin-up period.

4   Results

4.1   LPM simulations

335   The LPM is run over a certain range of temperature and vertical velocities, representative of the ACCACIA conditions. These ranges are determined by the 3D fields produced by the CNTRL simulation. Hourly outputs of the 3D LES fields indicate that the simulated cloud temperatures span from -6.5^{o}C to -1.5^{o}C; the coldest temperatures are found just below cloud top, while the cloud base temperature varies between -4°C and -2°C. The simulated updraft velocities in the cloud layer vary

340   between near-zero and ~1.4 m s^{-1}, while the mean W is 0.25 m s^{-1}. Following CNTRL results, the LPM is run for T_{cbh} between -5 and 0°C and vertical velocity, W, between 0.25 and 1.5 m s^{-1}, with a step value of 0.5^{o}C and 0.25 m s^{-1}, respectively, to derive the ice enhancement factors (Fig. 4).

Secondary ice processes are efficient in low updraft conditions, below 0.5 m s^{-1}, only when T_{cbh} is sufficiently cold (below -3°C), as warmer temperatures do not support the formation of large ice

345   particles. On the other hand, with increasing W, the lifetime of the parcel within the cloud layer becomes significantly shorter and does not allow for the ice crystals to rime sufficiently. As the simulations stop when the cloud temperature reaches -6.5^{o}C, the lowest simulated cloud top temperature (see Section 3.1), the duration of only those experiments with a somewhat warmer T_{cbh} is sufficient for ice particles to become large enough to initiate SIP. Within the range of T_{cbh} and W values that promote

350   large-particle formation, RS can enhance ice crystal concentrations by a factor of 2 to 10 (Fig. 4a), with the largest enhancements observed at low updraft conditions ($W<\sim 0.5$ m s^{-1}). For the same conditions, the enhancement from BR is about a factor of 30-40 (Fig. 4b), i.e. substantially larger than that due to RS. Generally, RS is considered more effective than BR within the -3 to -8°C temperature range (Yano and Phillips, 2011), but this is not the case for conditions that limit large-droplet formation, as those

355   examined here.

At higher velocities, combining BR and RS can result in ice enhancements similar to those from

BR alone; however, at lower updrafts the enhancement from the combination can be about two orders of magnitude larger (Fig. 4c). Substantial multiplication occurs only for conditions in which RS is somewhat more effective, enhancing ice concentrations by a factor of 3 or larger (Fig. 4a), because the ejected splinters can then grow to large sizes and result in more ice-ice collisions. Consequently, activating both mechanisms can lead to 3 times or more larger ice concentrations than only BR. However, when RS is weak, limited to about a 2-fold enhancement (Fig. 4a), BR dominates the whole multiplication process (Fig. 4b-c).

4.2 The impacts of SIP on cloud macrophysics and structure

Here the look-up tables of ice enhancement factors derived using the LPM is used, and CNTRL, RS, BR and ALLSIP LES simulations are compared to quantify the influence of the different SIP mechanisms on the Arctic stratocumulus. In the CNTRL simulation, primary ice formation results in ICNCs (N_{ice}) below the observed range (Fig. 5a), while the modeled mass mixing ratios (Q_{ice}) agree with only the lowest values observed (Fig. 5b). Activating RS enhances both N_{ice} and Q_{ice} by about a factor of 3 compared to the CNTRL simulation; however, the results still agree only with the lowest observed range of N_{ice} and Q_{ice}. Cloud ice content in BR, on the other hand, is about 25 (8.5) times larger than in the CNTRL (RS) simulation and in very good agreement with the observed median N_{ice} and Q_{ice} profiles. Activating both mechanisms in the ALLSIP simulation results in a 100-fold ice enhancement compared to CNTRL, which can account for the highest end of the measured values.

In our simulations, the RS process is found insufficient to explain the observed enhanced ice concentrations. The BR mechanism has been found in previous studies to be highly effective at producing ice at very cold temperatures (~ -15°C), resulting even in explosive multiplication (Yano and Phillips, 2011; 2016). Our results suggest that at relatively warmer temperatures and weak updraft conditions, BR acts as a weaker source of secondary ice, but it still significantly modulates the microphysical state of the cloud and can help explain the observed ice number and mass concentrations.

4.3 Sensitivity to CCN concentration

In this section, we examine the sensitivity of our results to the assumed CCN concentration. The LPM is run for two additional N_{CCN} conditions: 10, and 100 cm^{-3} and the results are shown in Fig. 6.

RS appears weaker with reduced CCN concentrations, as fewer large cloud droplets form to initiate this process (Figs. 4a and 6a,d), while BR is not affected by these variations (Figs. 4b and 6b,e). As a result, since in most thermodynamic conditions BR dominates the multiplication process, very little sensitivity is observed when all mechanisms are active (Figs. 4c and 5c,f). This is also reflected in Fig. 7, where the LES simulations are presented. While distinct differences are observed in cloud droplet concentrations in Fig. 7a, which are significantly reduced with decreasing N_{CCN}, cloud ice properties exhibit minor differentiations (Figs. 7b-c). This suggests that the main conclusions of this

study are not sensitive to the prescribed N_{CCN} conditions.

395 4.4 Sensitivity to INP concentration

Here we examine the sensitivity of our results to the INP concentration by testing two additional values: 0.01 L^{-1} and 1 L^{-1}. The LPM results are presented in Fig. 8, while the LES simulations are shown in Fig. 9.

A reduced INP number results in more effective RS (Figs. 4a and 8a,d). Since fewer ice crystals
400 are formed to compete with the liquid droplets for the available water vapor, more droplets can grow to large enough sizes to initiate RS. At the same time when INP=0.01 L^{-1}, the available ice crystals are very few to initiate break-up through collisions (Fig. 8b). As a result, this process appears effective only for very limited thermodynamic conditions, usually characterized by low updrafts ($W<\sim0.75$ m s^{-1}) and colder T_{cbh} ($< $-2°C); these conditions correspond to somewhat longer parcel lifetimes that allow only a
405 few ice crystals to grow to large sizes and initiate BR. However, once all mechanisms are activated, the new ice crystals generated by RS can further fuel BR; this is indicated by the fact that for a variety of thermodynamic conditions for which BR is inefficient (Fig. 8b), activating both mechanisms simultaneously (Fig. 8c) results in larger ice enhancements than having only RS active (Fig. 8a). 'BR' and 'ALL SIP' LPM simulations show little sensitivity to varying INP concentrations between 0.1-1 L^{-}
410 ^{1}.

When implementing the LPM results of Fig. 8 in the LES model, distinct differences are observed in the produced cloud ice properties (Fig. 9). The INP0.01 simulation hardly produces any ice if no SIP is accounted for (Fig. 9b, c). Activating SIP results in ice properties similar to the lowest values observed. Similarly, when INP=0.1 L^{-1} the results fall within the observed range only when SIP
415 is activated. For extremely high INP conditions, the INP1 simulation can reproduce the median observed concentration (Fig. 9b) with primary nucleation. Further ice production in INP1_SIP results in glaciation of the largest portion of the cloud (Fig. 9a), while very few liquid droplets remain concentrated in a thin layer about 100-m deep. Yet SIP has no significant impact on the cloud ice properties; the produced ICNCs remain within the observed range (Fig. 9b) for the rest of the simulation
420 time, while the ice mass mixing ratio is only slightly larger and in better agreement with median observed profile (Fig. 9c).

These sensitivity simulations indicate that including a SIP description in our model results in generally better representation of the cloud ice properties for a variety of INP conditions. All simulations that account for SIP, including the sensitivity test with the unrealistically high INP
425 concentration, reproduce cloud ice properties within the observed range.

5. Discussion and conclusions

Semi-idealized simulations of Arctic stratocumulus clouds observed during the ACCACIA campaign

430   are performed to investigate the impact SIP using a LES and a LPM: the LES provides a realistic representation of the atmospheric thermodynamics, while the LPM provides a more simplified framework to parameterize SIP. Our simulations indicate that DS remains inactive in the cold Arctic conditions. RS is very weak due to the limited concentration of large drops, while BR is the only mechanism that can sufficiently explain the observed ICNCs.

The inefficiency of DS is in good agreement with previous studies, which indicate that a

435   relatively warm cloud base temperature is critical for the initiation of DS (Lawson et al., 2017; Sullivan et al., 2018a). The limited influence of RS in clouds with very few large raindrops to initiate this process is also quite conceivable. RS has also been found insufficient to explain the observed ICNCs in Antarctic stratocumulus clouds of similar temperature in Weather and Research Forecasting (WRF) simulations conducted by Young et al. (2019). To reproduce the observations, they had to remove from

440   the RS parameterization the liquid thresholds that allow RS activation only when sufficiently large droplets are formed, and, further multiply the RS splinter production efficiency by a factor of 10.

Our results here indicate that at relatively warm sub-zero temperatures and in low updraft conditions that do not favor the formation of large raindrops, BR is a potentially important mechanism. Interestingly, if BR is excluded from our simulations, the RS effect should be multiplied with a factor of

445   10 to obtain a good agreement with the observed ICNCs, i.e. the factor as in Young et al. (2019). However we acknowledge that the magnitude of the BR efficiency highly depends on some of the adapted assumptions: (a) SIP is considered to be favored by updraft conditions only, neglecting possible collisions in downdrafts which can further enhance ice multiplication. (b) BR effect is highly dependent on τ_g (Yano and Phillips 2011), a parameter that cannot be objectively defined; here its empirical

450   definition is based on the observations (See Section 3.2 for a discussion). A shorter τ_g will likely enhance BR as the new fragments can rapidly grow to large sizes that further fuel this process. On the other hand, a longer τ_g may prevent ice particles from growing to sizes large enough to initiate SIP. Nevertheless, the observations reveal a broad spectrum of crystal sizes (Fig. S3), often large enough (up to 1.27 mm) to potentially initiate BR. (d) The description used to parameterize the BR effect by

455   Takahashi et al. (1995) is subject to great uncertainty. These experiments used direct collisions, while changes in the collision angle may impact the fragment number produced. Furthermore, one of the two colliding hydrometeors remained fixed; in reality, the relative velocity of the two hydrometeors sedimenting out or tumbling within turbulent motions may yield different fragmentation numbers. An extensive discussion on the limitations of these experimental set-ups can be found in Phillips et al.

460   (2017a).

Evidence of collisional break-up has been documented in observations of Arctic mixed-phase clouds in the past (Rangno and Hobbs, 2001; Schwarzenboeck et al., 2009). However, very few attempts have been made to incorporate this process in mesoscale models and climate models. A main challenge in parameterizing BR is that a correct spectral representation of the ice crystals is required,

465   which is more feasible in bin microphysics schemes (e.g. Phillips et al. 2017b). However, bin microphysics are computationally expensive and most weather forecast and climate models incorporate bulk microphysical representations.

        Hoarau et al. (2018) recently incorporated BR in a mesoscale model which included a two-moment microphysics scheme with three ice hydrometeor types: ice crystal, graupel and snow particles,
470   whose sizes are determined by gamma distributions (as in most bulk schemes). To represent BR, they assumed that this process occurs only when snow collides with graupel and the new fragments are added to the ice crystal category. However, this approach may result in significantly underestimated SIP as other type of collisions that include large ice crystals may occur (Phillips et al. 2017a). Sullivan et al. (2018b) did consider collisions between ice crystals and the other two hydrometeor types in a similar
475   bulk scheme in COSMO-ART. However, their approach may instead result in an overestimated BR efficiency, as not all crystal sizes are suitable to fuel this process, including the very small fragments generated by BR.

        It is likely that a property-based ice microphysics scheme, like the Predicted Particle Properties (P3) scheme (Morrison and Milbrandt, 2015; Milbrandt and Morrison, 2016) in WRF, can support a
480   more realistic representation of the BR process. This scheme tracks ice mixing ratio, number, mass, and rime fraction rather than number and mass in snow, graupel, and ice crystal categories whose thresholds can be non-physical. However, in the current version of WRF, it considers only two ice categories while at least three are needed for the BR description (see Section 4.2 for a discussion). Nevertheless, one of the most important outcomes of the study is that the simple framework of the LPM, when driven
485   ("tuned") by the conditions relevant for the LES simulations – despite the complexity and variability of the latter -, provides ice number enhancement factors that bridge the LES with observations. This suggests that the LPM, when appropriately constrained from observations (or LES-type simulations), provides a promising approach towards parameterizing SIP in large-scale models.

        Our results indicate that BR is likely a critical mechanism in Arctic stratocumulus clouds, where
490   large drops are sparse and RS efficiency is limited. Thus a correct representation of this process in models will likely alleviate some of the model deficiencies in representing cloud ice properties and hence the shortwave radiation budget (Young et al., 2019). As there have been significant advances in the development of laboratory instruments suitable for BR studies through the past decades, we highlight the need for new laboratory experiments with more realistic set-ups that focus on the BR
495   mechanism. We believe that constraining BR accurately in models could have a significant impact on the projection of the future Arctic climate.

        Code availability: The LPM code can be found on https://github.com/scs2229/SIM. The LES code is available upon request.

500

Data availability: ACCACIA observations are available on https://data.bas.ac.uk and http://www.ceda.ac.uk.

Author contribution: AN and GS conceived and lead this study. AMLE and JS provided the LES
505 code, while SS wrote the original LPM code. GL and TLC provided the ACCACIA observations. GS performed the LPM and LES simulations, analyzed the results, and together with AN wrote the main manuscript. AMLE, SS and JS were also involved in the scientific interpretation, discussion, and commented on the paper.

510 **Competing interests:** The authors declare that they have no conflict of interest.

Acknowledgements: We acknowledge support from Laboratory of Atmospheric Processes and Their Impacts at the Ecole Polytechnique Federale de Lausanne, Switzerland (http://lapi.epfl.ch) and the project PyroTRACH (ERC-2016-COG) funded by H2020-EU.1.1. – Excellent Science – European
515 Research Council (ERC), project ID 726165. We are also grateful to ACCACIA scientific crew for the observational datasets used in this study.

References:

Barton, N. P., S. A. Klein, and Boyle, J. S.: On the Contribution of Longwave Radiation to Global
520 Climate Model Biases in Arctic Lower Tropospheric Stability. J. Clim., 27, 7250-7269, doi: 10.1175/JCLI-D-14-00126.1, 2014.

Bogacki, P., and Shampine, L. F.: A 3(2) pair of Runge-Kutta formulas, Appl. Math. Letters, 2, 321–325, doi:10.1016/0893-9659(89)90079-7, 1989.

525

Brown, P. and Francis, P.: Improved measurements of the ice water content in cirrus using a total-water probe, J. Atmos. Ocean. Tech, 12, 410–414, 1995.

Choularton, T. W., D. J. Griggs, B. Y. Humood, and Latham, J. : Laboratory studies of riming, and its
530 relation to ice splinter production. Quart. J. Roy. Meteor. Soc., 106, 367–374, doi:https://doi.org/10.1002/qj.49710644809, 1980.

Crawford, I., Bower, K. N., Choularton, T. W., Dearden, C., Crosier, J., Westbrook, C., Capes, G., Coe, H., Connolly, P. J., Dorsey, J. R., Gallagher, M. W., Williams, P., Trembath, J., Cui, Z., and Blyth, A.:

535 Ice formation and development in aged, wintertime cumulus over the UK: observations and modelling, Atmos. Chem. Phys., 12, 4963-4985, https://doi.org/10.5194/acp-12-4963-2012, 2012.

Crosier, J., Choularton, T. W., Westbrook, C. D., Blyth, A. M., Bower, K. N., Connolly, P. J., Dearden, C., Gallagher, M. W., Cui, Z., and Nicol, J. C.: Microphysical properties of cold frontal rainbands, Q. J.
540 Roy. Meteorol. Soc., 140, 1257–1268, doi:10.1002/qj.2206, 2013.

DeMott, P. J., Prenni, A. J., Liu, X., Kreidenweis, S. M., Petters, M. D., Twohy, C. H., Richardson, M. S., Eidhammer, T., and Rogers, D. C.: Predicting global atmospheric ice nuclei distributions and their impacts on climate, Proc. Nat. Acad. Sci., doi:10.1073/pnas.0910818107, 2010.

545

Durran, D.R.: Numerical Methods for Fluid Dynamics, Texts Appl. Math., 2nd ed., Springer, Berlin-Heidelberg, Germany, 2010.

Field, P., Lawson, P., Brown, G., Lloyd, C., Westbrook, D., Moisseev, A., Miltenberger, A., Nenes, A.,
550 Blyth, A., Choularton, T., Connolly, P., Bühl, J., Crosier, J., Cui, Z., Dearden, C., DeMott, P., Flossmann, A., Heymsfield, A., Huang, Y., Kalesse, H., Kanji, Z., Korolev, A., Kirchgaessner, A., Lasher-Trapp, S., Leisner, T., McFarquhar, G., Phillips, V., Stith, J., and Sullivan, S.: Chapter 7: Secondary ice production - current state of the science and recommendations for the future, Meteor. Monogr., doi:10.1175/AMSMONOGRAPHS-D-16-0014.1, 2017.

555

Fridlind, A. M., Ackerman, A. S., McFarquhar, G., Zhang, G., Poellot, M. R., DeMott, P. J., Prenni, A. J., and Heymsfield, A. J.: Ice properties of single-layer stratocumulus during the Mixed-Phase Arctic Cloud Experiment: 2. Model results., J. Geophys. Res., 112, D24202, https://doi.org/10.1029/2007JD008646, 2007.

560

Fu, Q, and Liou K.N: On the Correlated k-Distribution Method for Radiative Transfer in Nonhomogeneous Atmospheres, J. Atmos., 49(22): 2139–2156, doi: 10.1007/s00382-016-3040-8, 1992

Gayet, J.-F., Treffeisen, R., Helbig, A., Bareiss, J., Matsuki, A., Herber, A., and Schwarzenboeck,
565 A.: On the onset of the ice phase in boundary layer Arctic clouds, J. Geophys. Res., 114, D19201, doi:10.1029/2008JD011348, 2009

Gettelman, A., Liu, X., Ghan, S. J., Morrison, H., Park, S., Conley, A. J., Klein, S. A., Boyle, J., Mitchell, D. L., and F. Li, J.-L.: Global simulations of ice nucleation and ice supersaturation with an

570   improved cloud scheme in the Community Atmosphere Model, J. Geophys. Res., 115, D18216, doi:10.1029/2009JD013797, 2010.

Hallett, J. and Mossop, S. C.: Production of secondary ice particles during the riming process, Nature, 249, 26–28, doi:10.1038/249026a0, 1974.

575

Hoarau, T., Pinty, J.-P., and Barthe, C.: A representation of the collisional ice break-up process in the two-moment microphysics LIMA v1.0 scheme of Meso-NH, Geosci. Model Dev., 11, 4269-4289, https://doi.org/10.5194/gmd-11-4269-2018, 2018.

580   Heymsfield, A. J., and Mossop, S. C.: Temperature dependenceof secondary ice crystal production during soft hailgrowth by riming. Quart. J. Roy. Meteor. Soc., 110, 765–770,doi:10.1002/qj.49711046512, 1984

Jensen, A. A. and Harrington J. Y.: Modeling ice crystal aspect ratio evolution during riming: A single-
585   particle growth model. J. Atm. Sci., 72, 2569-2590, doi: 10.1175/JAS-D-14-0297.1, 2015.

Jones, H. M., Young, G., Choularton, T. W., Bower, K. N., Lachlan-Cope, T., O'Shea, S., Dorsey, J., Ladkin, R., Kirchgaessner, A., and Weiss, A.: Summertime Arctic Aircraft Measurements during ACCACIA, Atmos. Chem. Phys. Discuss., https://doi.org/10.5194/acp-2018-283, 2018.

590

Jung, C.H., Yoon, Y.J., Kang, H.J., Gim, Y., Lee, B.Y., Ström, J., Krejci, R. and Tunved, P.: The seasonal characteristics of cloud condensation nuclei (CCN) in the arctic lower troposphere, Tellus B: Chemical and Physical Meteorology ,70:1, 1-13, DOI: 10.1080/16000889.2018.1513291, 2018.

595   Karlsson, J., and Svensson, G. Consequences of poor representation of Arctic sea-ice albedo and cloud-radiation interactions in the CMIP5 model ensemble, Geophys. Res. Lett., 40, 4374–4379, doi:10.1002/grl.50768, 2013.

Korolev, A., McFarquhar, G., Field, P.R., Franklin, C., Lawson, P., Wang, Z., Williams, E., Abel, S.J.,
600   Axisa, D., Borrmann, S., Crosier, J., Fugal, J., Krämer, M., Lohmann, U., Schlenczek, O., Schnaiter, M., and Wendisch, M.: Mixed-Phase Clouds: Progress and Challenges. Meteorological Monographs, 58, 5.1–5.50, https://doi.org/10.1175/AMSMONOGRAPHS-D-17-0001.1, 2017.

Korolev, A. V., Emery, E. F., Strapp, J.W., Cober, S. G., Isaac, G. A., Wasey, M., and Marcotte, D.:
605   Small ice particles in tropospheric clouds: fact or artifact?, B. Am. Meteorol. Soc., 92, 967–973,

doi:10.1175/2010BAMS3141.1, 2011.

Korolev, A. V., Emergy, E., and Creelman, K.: Modification and Tests of Particle Probe Tips to Mitigate Effects of Ice Shattering, J. Atmos. Ocean. Tech., 30, 690–708, 2013.

610

Lauber, A., Kiselev, A., Pander, T., Handmann, P., and Leisner, T.: Secondary ice formation during freezing of levitated droplets, J. Atmos. Sci., 75, 2815–2826, https://doi.org/10.1175/JAS-D-18-0052.1, 2018.

Lawson, R. P.,Woods, S., and Morrison, H.: The microphysics of ice and precipitation development in

615   tropical cumulus clouds, J. Atm. Sci.,72, 2429–2445, doi:10.1175/JAS-D-14-0274.1, 2015.

Lawson, P., Gurganus, C., Woods, S., and Bruintjes, R.: Aircraft observations of cumulus microphysics ranging from the tropics to midlatitudes: implications for a "new" secondary ice process, J. Atmos. Sci., 74, 2899–2920, https://doi.org/10.1175/JAS-D-17-0033.1, 2017.

620

Leisner, T., Pander, T., Handmann, P., and Kiselev, A.: Secondary ice processes upon heterogeneous freezing of cloud droplets, 14th Conf. on Cloud Physics and Atmospheric Radiation, Amer. Meteor. Soc, Boston, MA, 2014.

625   Li, G., Wang, Y., and Zhang, R.:Implementation of a two-moment bulk microphysics scheme to the WRF model to investigate aerosol - cloud interaction, J. Geophys. Res., 113, D15211, doi:10.1029/2007JD009361, 2008.

Lilly, D.K.: A proposed modification to the Germano subgrid-scale closure method, Phys. Fluids, 4:

630   633–635, doi:10.1063/1.858280, 1992.

Lloyd, G., Choularton, T. W., Bower, K. N., Gallagher, M. W., Connolly, P. J., Flynn, M., Farrington, R., Crosier, J., Schlenczek, O., Fugal, J., and Henneberger, J.: The origins of ice crystals measured in mixed-phase clouds at the high-alpine site Jungfraujoch, Atmos. Chem. Phys., 15, 12953–

635   12969, https://doi.org/10.5194/acp-15-12953-2015, 2015.

Mignani, C., Creamean, J. M., Zimmermann, L., Alewell, C., and Conen, F.: New type of evidence for secondary ice formation at around −15 °C in mixed-phase clouds, Atmos. Chem. Phys., 19, 877-886, https://doi.org/10.5194/acp-19-877-2019, 2019.

640   Milbrandt, J.A. and Morrison, H.: Parameterization of Cloud Microphysics Based on the Prediction of Bulk Ice Particle Properties. Part III: Introduction of Multiple Free Categories. J. Atmos. Sci., 73, 975–995, https://doi.org/10.1175/JAS-D-15-0204.1, 2016.

Mossop, S. C.: Production of secondary ice particles during the growth of graupel by riming. Q.J.R.
645   Meteorol. Soc., 102: 45-57. doi:10.1002/qj.49710243104, 1976.

Mossop, S. C., and Hallett, J.: Ice crystal concentration in cumulus clouds: Influence of the drop spectrum. Science, 186, 632–634. https://doi.org/10.1126/science.186.4164.632, 1974.

650   Morrison, H. and Milbrandt, J.A.: Parameterization of Cloud Microphysics Based on the Prediction of Bulk Ice Particle Properties. Part I: Scheme Description and Idealized Tests. J. Atmos. Sci., 72, 287–311, https://doi.org/10.1175/JAS-D-14-0065.1, 2015.

Morrison, H., Zuidema, P., Ackerman, A.S., Avramov, A., de Boer, G., Fan, J., Fridlind, A.M.,
655   Hashino, T., Harrington, J.Y., Luo, Y., Ovchinnikov, M., and Shipway, B.: Intercomparison of cloud model simulations of Arctic mixed-phase boundary layer clouds observed during SHEBA/FIRE-ACE, J. Adv. Model. Earth Syst., 3, M06003, doi:10.1029/2011MS000066, 2011.

Paukert, M., Hoose, C., and Simmel, M.: Redistribution of ice nuclei between cloud and rain droplets:
660   parameterization and application to deep convective clouds, J. Adv. Model. Earth Sy., 9, 514–535, https://doi.org/10.1002/2016MS000841, 2017.

Persson, P.O.G, Fairall, C.W., Andreas, E.L., Guest, P.S., and Perovich, D.K: Measurements near the atmospheric surface flux group tower at SHEBA: Near-surface conditions and surface energy budget, J.
665   Geophys. Res., 107(C10): 8045, doi:10.1029/2000JC000705, 2002.

Phillips, V. T. J., Yano, J.-I., and Khain, A.: Ice multiplication by breakup in ice-ice collisions. Part I: Theoretical formulation, J. Atmos. Sci., 74, 1705–1719, https://doi.org/10.1175/JAS-D-16-0224.1, 2017a.

670   Phillips, V.T., Yano, , J.-I., Formenton, M., Ilotoviz, E., Kanawade, V., Kudzotsa, I., Sun, J., Bansemer, A., Detwiler, A.G., Khain, A., and Tessendorf, S.A.: Ice Multiplication by Breakup in Ice–Ice Collisions. Part II: Numerical Simulations. J. Atmos. Sci., 74, 2789–2811, https://doi.org/10.1175/JAS-D-16-0223.1, 2017b.

675 Phillips, V.T., S. Patade, J. Gutierrez, and A. Bansemer: Secondary Ice Production by Fragmentation of Freezing Drops: Formulation and Theory. *J. Atmos. Sci.,* 75, 3031–3070, https://doi.org/10.1175/JAS-D-17-0190.1, 2018.

Rangno, A. L., and Hobbs, P. V.: Ice particles in stratiform clouds in the Arctic and possible
680 mechanisms for the production of high ice concentrations, J. Geophys. Res., 106, 15,065–15,075, doi:10.1029/2000JD900286, 2001.

Rosenbrock, H. H.: Some general implicit processes for the numerical solution of differential equations, The Comp. Jour., 5(4), 329–330, doi:10.1093/comjnl/5.4.329,1963.
685
Savre, J, Ekman, AML, and Svensson, G.: Technical note: Introduction to MIMICA, a large-eddy simulation solver for cloudy planetary boundary layers, J. Adv. Model. Earth Syst., 6, doi:10.1002/2013MS000292, 2015.

690 Schwarzenboeck, A., Shcherbakov,V., Lefevre, R., Gayet, J.-F., Duroure, C., and Pointin, Y.: Evidence for stellar-crystal fragmentation in Arctic clouds,Atmos. Res.,92, 220–228, doi:10.1016/j.atmosres.2008.10.002, 2009.

Sedlar, J, Tjernström, M., Mauritsen, T., Shupe, M. D., Brooks, I. M., Persson, P. O. G., Birch, C. E.,
695 Leck, C., Sirevaag, A., and Nicolaus, M.: A transitioning Arctic surface energy budget: the impacts of solar zenith angle, surface albedo and cloud radiative forcing, Clim. Dynam., 37, 1643–1660, doi:10.1007/s00382-010-0937-5, 2011.

Seifert, A., and Beheng. K. D: A double-moment parameterization for simulating auto conversion,
700 accretion and self collection, Atmos. Res., 59–60: 265–281, doi:10.1016/S0169-8095(01)00126-0, 2001.

Shupe, M. D. and Intrieri, J. M.: Cloud radiative forcing of the Arcticv surface: The influence of cloud properties, surface albedo, and solar zenith angle, J. Climate, 17, 616–628, doi:10.1175/1520-
705 0442(2004)017<0616:CRFOTA>2.0.CO;2, 2004.

Shupe, M. D., Walden, V. P., Eloranta, E., Uttal, T., Campbell, J. R., Starkweather, S. M., and Shiobara, M.: Clouds at Arctic Atmospheric Observatories, Part I: Occurrence and macrophysical properties, J. Appl. Meteor. Clim., 50, 626–644,
710 doi:10.1175/2010JAMC2467.1, 2011.

Sotiropoulou, G., Sedlar, J., Forbes, R., and Tjernström, M.: Summer Arctic clouds in the ECMWF forecast model: an evaluation of cloud parametrization schemes. Quart. J. Roy. Meteorol. Soc., 142, 387–400, doi: 0.1002/qj.2658, 2016.

715

Storelvmo, T., Kristjánsson, J.E., and Lohmann, U.: Aerosol Influence on Mixed-Phase Clouds in CAM-Oslo. J. Atmos. Sci., 65, 3214–3230, https://doi.org/10.1175/2008JAS2430.1, 2008.

Sullivan, S., Hoose, C., and Nenes, A.: Investigating the contribution of secondary production to ice

720 crystal number concentrations, J. Geophys. Res., doi:10.1002/2017JD026546, 2017.

Sullivan, S. C., Kiselev, A., Leisner, T., Hoose, C., and Nenes, A.: Initiation of secondary ice production in clouds, Atmos. Chem. Phys., 18, 1593–1610, doi:10.5194/acp-18-1593-2018, 2018a.

725 Sullivan, S. C., Barthlott, C., Crosier, J., Zhukov, I., Nenes, A., and Hoose, C.: The effect of secondary ice production parameterization on the simulation of a cold frontal rainband, Atmos. Chem. Phys., 18, 16461–16480, https://doi.org/10.5194/acp-18-16461-2018, 2018b.

Takahashi, T., Nagao, Y., and Kushiyama, Y.: Possible high ice particle production during graupel-

730 graupel collisions, J. Atmos. Sci., 52, 4523–4527, doi:10.1175/1520-0469, 1995.

Vardiman, L.: The generation of secondary ice particles in clouds by crystal-crystal collision, J. Atmos. Sci., 35, 2168–2180, doi:10.1175/1520-0469, 1978.

735 Wang, C., and J. Chang, J.: A three-dimensional numerical model of cloud dynamics, microphysics, and chemistry. 1: Concepts and formulation, J. Geophys. Res., 98, 16,787–16,798, doi:10.1029/92JD01393, 1993.

Wildeman, S., Sterl, S., Sun, C., and Lohse, D.: Fast dynamics of water droplets freezing from the

740 outside in, Phys. Rev. Lett., 118, doi:10.1103/PhysRevLett.118.084101, 2017.

Williams, P.D.: The RAW filter: An improvement to the Robert-Asselin filter in semi-implicit integrations, Mon. Weather Rev., 139: 1996–2007, doi:10.1175/2010 MWR3601.1, 2010.

745 Yano, J.-I. and Phillips, V. T. J.: Ice-ice collisions: an ice multiplication process in atmospheric clouds,

J. Atmos. Sci., 68, 322–333, doi:10.1175/2010JAS3607.1, 2011.

Yano, J.-I., Phillips, V. T. J., and Kanawade, V.: Explosive ice multiplication by mechanical break-up in-ice-ice collisions: a dynamical system-based study, Q. J. Roy. Meteor. Soc., 142, 867–879,
750   https://doi.org/10.1002/qj.2687, 2015.

Young, G., Jones, H. M., Darbyshire, E., Baustian, K. J., McQuaid, J. B., Bower, K. N., Connolly, P. J., Gallagher, M. W., and Choularton, T. W.: Size-segregated compositional analysis of aerosol particles collected in the European Arctic during the ACCACIA campaign, Atmos. Chem. Phys., 16, 4063-4079,
755   https://doi.org/10.5194/acp-16-4063-2016, 2016.

Young, G., Lachlan-Cope, T., O'Shea, S. J., Dearden, C., Listowski, C., Bower, K. N., Choularton T.W., and Gallagher M.W.: Radiative effects of secondary ice enhancement in coastal Antarctic clouds. *Geophysical Research Letters*, 46, 23122321. , https://doi.org/10.1029/2018GL080551, 2019.

760

Wesslén, C., M. Tjernström, D. H. Bromwich, G. de Boer, A. M. L. Ekman, L. S. Bai, and S. H. Wang, 2014: The Arctic summer atmosphere: an evaluation of reanalyses using ASCOS data. Atmos. Chem. Phys., 14, 2605-2624, doi:10.5194/acp-14-2605-2014.

765

Wex, H., Huang, L., Zhang, W., Hung, H., Traversi, R., Becagli, S., Sheesley, R. J., Moffett, C. E., Barrett, T. E., Bossi, R., Skov, H., Hünerbein, A., Lubitz, J., Löffler, M., Linke, O., Hartmann, M., Herenz, P., and Stratmann, F.: Annual variability of ice-nucleating particle concentrations at different Arctic locations, Atmos. Chem. Phys., 19, 5293-5311, https://doi.org/10.5194/acp-19-5293-2019, 2019.

Table 1: Description of the LES experiments performed in this study

LES experiment	SIP process activated	CCN concentration (cm^{-3})	INP concentration (L^{-1})
CNTRL	none	50	0.1
RS	rime-splintering	50	0.1
BR	collisional break-up	50	0.1
ALLSIP	all	50	0.1
CCN10	none	10	0.1
CCN100	none	100	0.1
CCN10_SIP	all	10	0.1
CCN100_SIP	all	100	0.1
IN0.01	none	50	0.01
IN1	none	50	1
IN0.01_SIP	all	50	0.01
IN1_SIP	all	50	1

Figures:
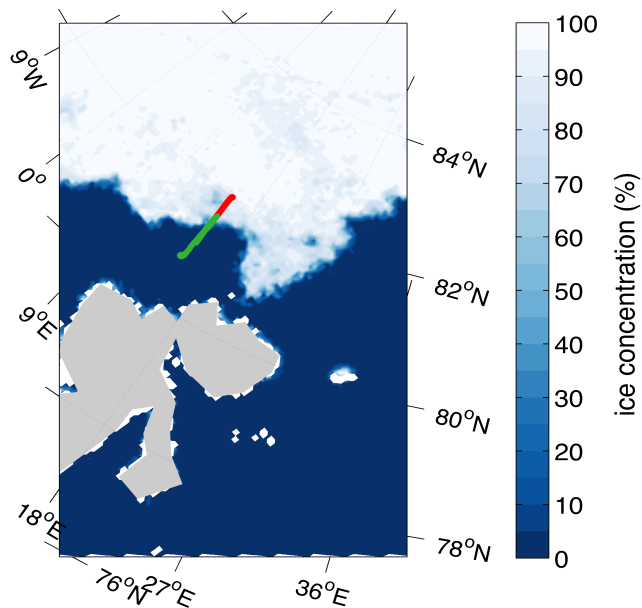
Figure 1. Advanced Microwave Scanning Radiometer (AMSR2) daily sea-ice concentrations (grid resolution 6.25 km), from University of Bremen, for 23 July 2013. Green line represents the flight track during ACCACIA campaign, between 10-11 UTC. Red line shows the flight track at latitudes > 81.7°N; measurements collected along this track are used to evaluate the simulated cloud properties.
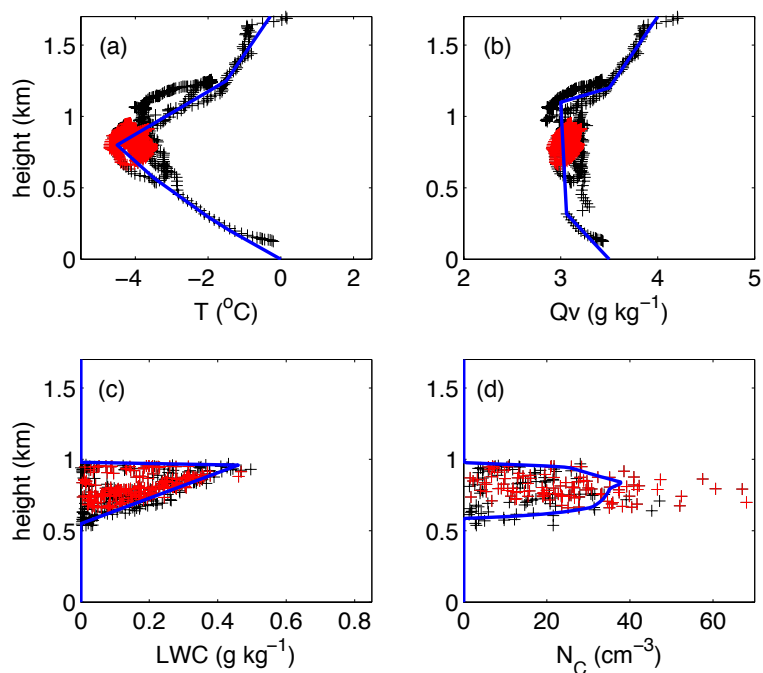
Figure 2: Measurements of (a) temperature (°C), (b) specific humidity (g kg^{-1}) and (c) liquid water content (g kg^{-1}) collected on 23 July 2013 (10-11 UTC) are indicated with black crosses. Red crosses indicate the measurements collected over the ice-pack (above 81.7°N); these are used to evaluate the simulated cloud properties. The blue lines in panels (a-c) represent the simplified vertical profiles used to initialize the LES, while in panel (d) it indicates the cloud droplet concentrations generated by the LES with CCN activation after 1 hour of simulation.
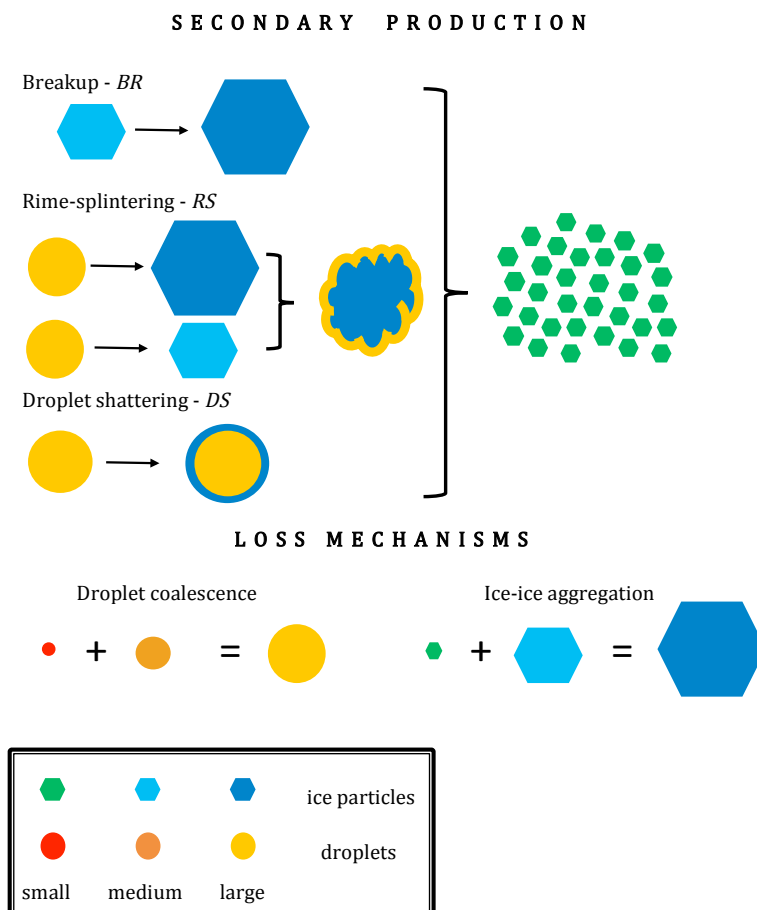
Figure 3: Schematic representation of the simplified six-bin microphysics (adopted from Sullivan et al. 2017)
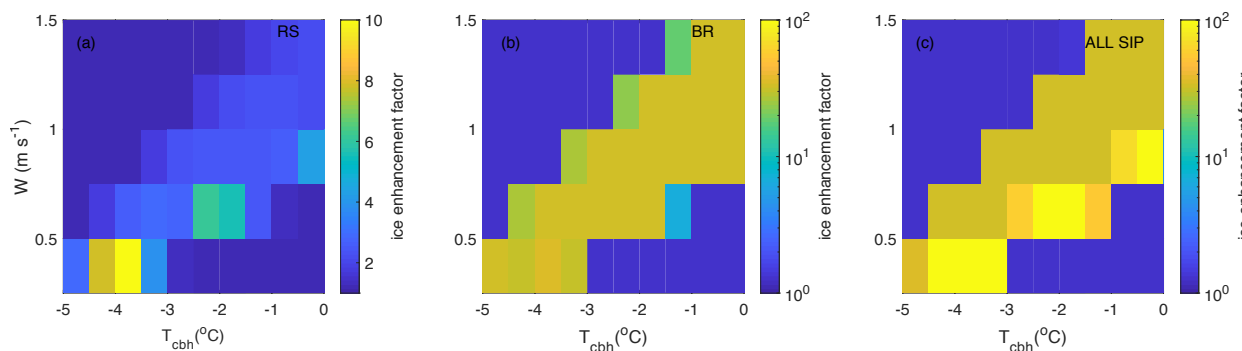
Figure 4: Enhancement factors for ice crystal number concentrations (N_i) as a function of updraft velocity (W) and cloud base temperature (T_{cbh}). The different panels correspond to the LPM simulations in which (a) rime-splintering (RS), (b) break-up upon ice-ice collisions (BR), (c) all SIP mechanisms are active. These results are used as look-up tables in the LES to parameterize secondary ice production. Note the logarithmic scale of the colorbars in panels (b) and (c).
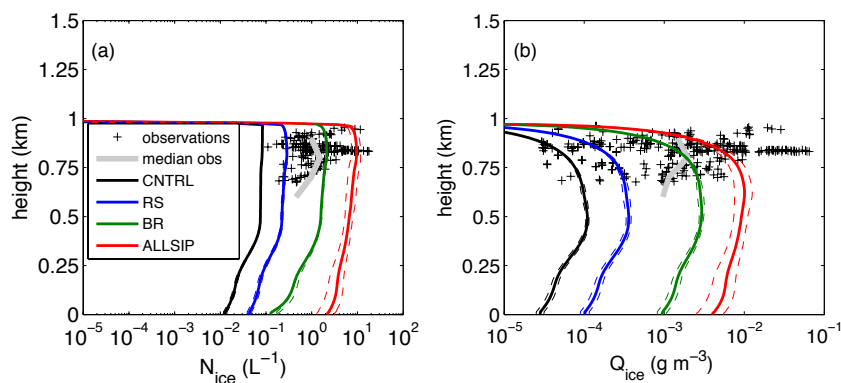
Figure 5: Vertical profiles of (a) ice crystal number concentration (N_{ice}) and (b) ice mass mixing ratio (Q_{ice}) for CNTRL (black), RS (blue), BR (green) and ALLSIP (red) from the LES. Solid lines represent the mean profiles, averaged between 4-8 hours of simulation time, while dashed lines show the standard deviation. Black crosses represent the measurement range derived from the 2D-S Probe, while grey lines represent the observed median profiles.
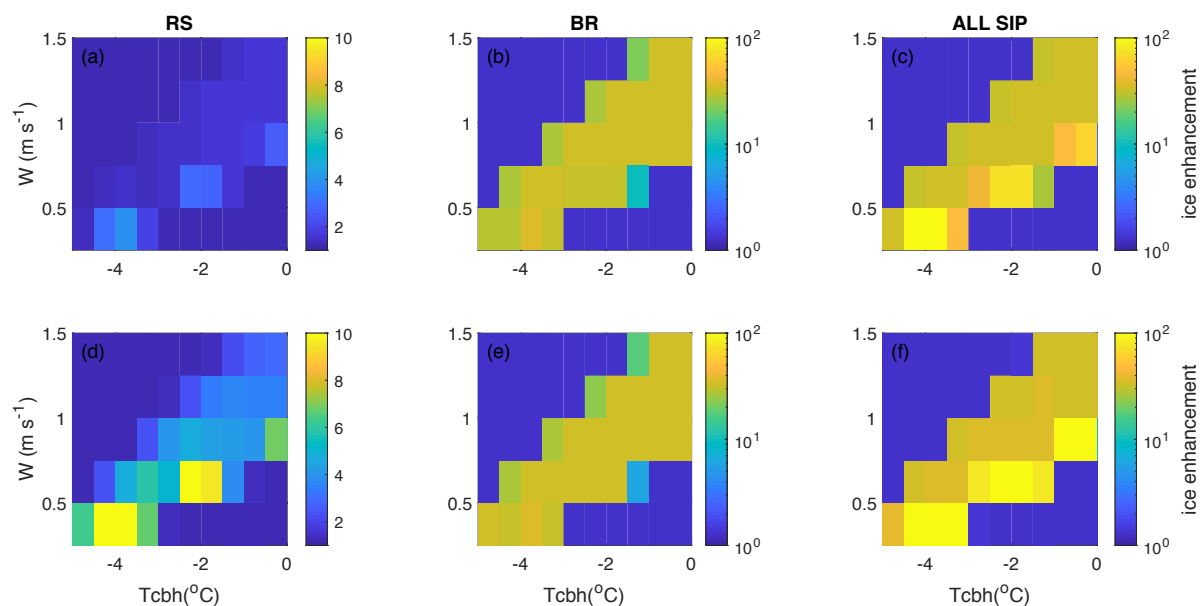
Figure 6: Same as Fig. 4 but for the LPM simulations with varying N_{CCN} concentrations: (a-c) 10 cm^{-3} and (d-f) 100 cm^{-3}. The three columns correspond to three different set-ups: (a, d) rime-splintering, (b, e) break-up upon ice-ice collisions, and (c, f) all SIP mechanisms are activated.
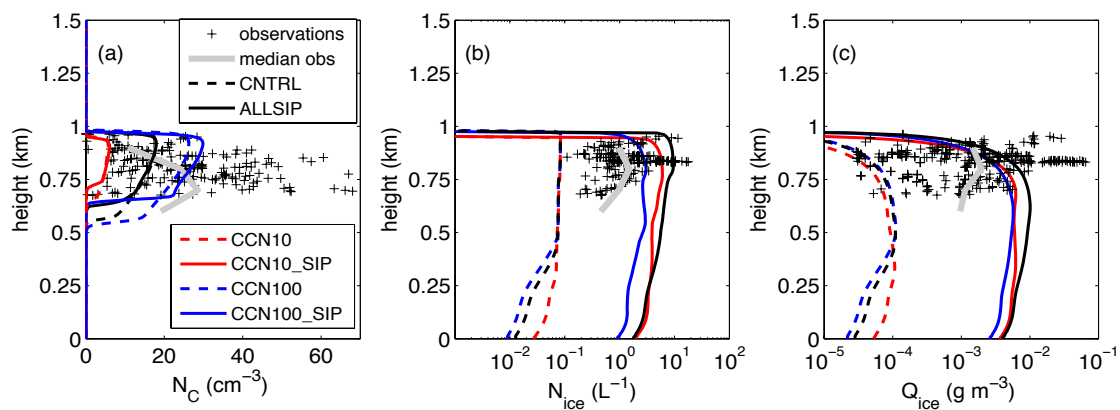
Figure 7: Vertical profiles of (a) cloud droplet concentrations (cm^{-3}), (b) ice crystal concentrations (L^{-1}) and (c) ice mass mixing ratio (g m^{-3}) for the LES sensitivity simulations with varying N$_{CCN}$. Black, red and blue dashed (solid) lines represent CNTRL (ALLSIP), CCN10 (CCN10_SIP) and CCN100 (CCN100_SIP) runs, respectively. The results are averaged between 4-8 hours of simulation time. Black crosses represent the observations, while the solid grey lines show the median observed profile.
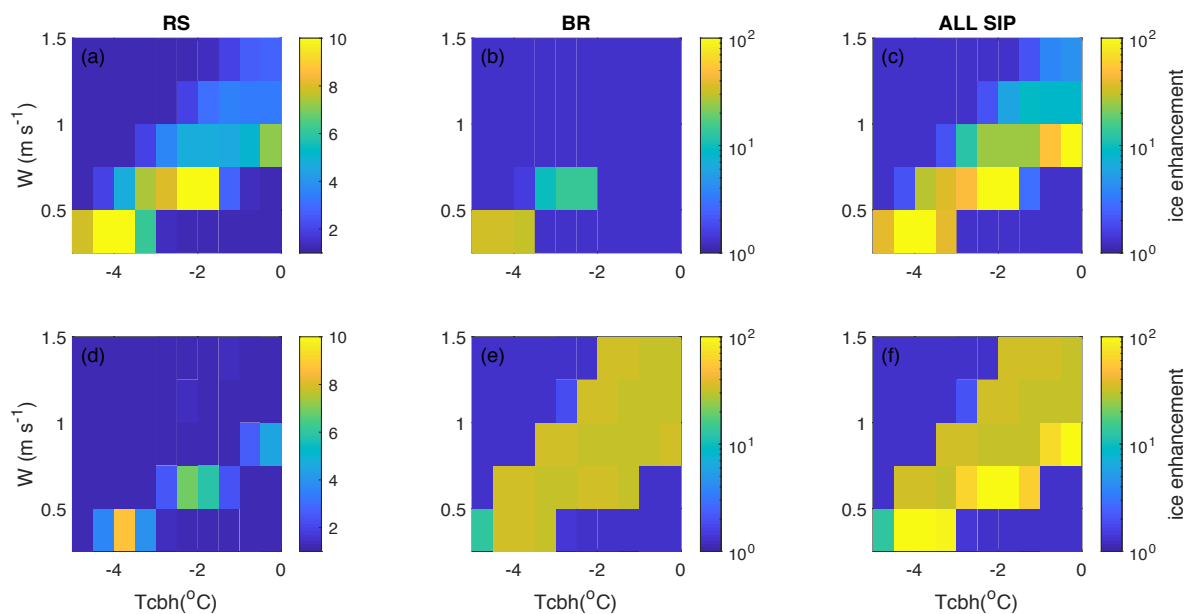
Figure 8: Same as Fig. 6 but for LMP simulations with varying INP concentrations: (a-c) 0.01 L^{-1} and (d-f) 1 L^{-1}.
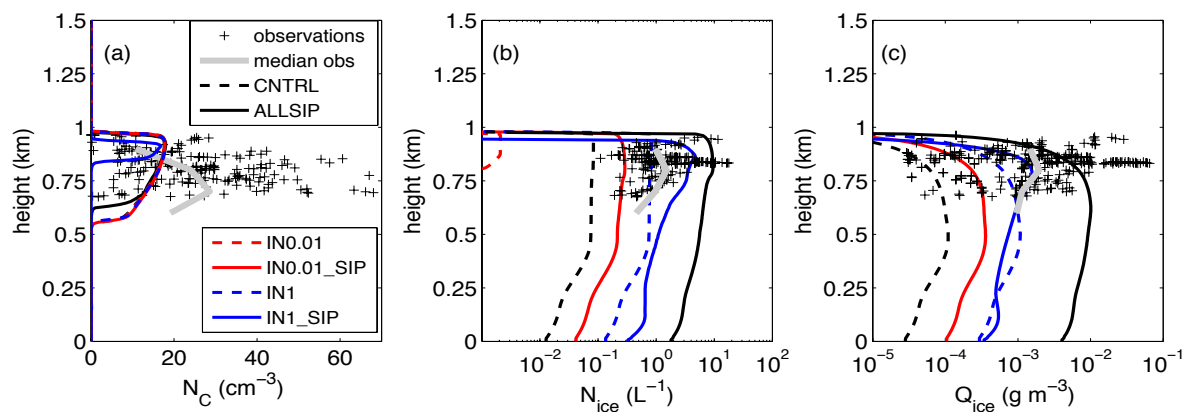
Figure 9: Same as Fig. 7 but for the LES sensitivity simulations with varying INP concentration. Black, red and blue dashed (solid) lines represent CNTRL (ALLSIP), IN0.01 (IN0.01_SIP) and IN1 (IN1_SIP) runs, respectively.